JVST B
Journal of Vacuum Science & Technology B

# Effectiveness of multipass and multirow writing methods for massively parallel e-beam systems

Cite as: J. Vac. Sci. Technol. B **38**, 062601 (2020); https://doi.org/10.1116/6.0000547
Submitted: 13 August 2020 • Accepted: 18 September 2020 • Published Online: 02 October 2020

**Md Nabid Hasan, Soo-Young Lee, Byung-Sup Ahn, et al.**

JVST B
Journal of Vacuum Science & Technology B

ARTICLE

avs.scitation.org/journal/jvb

# Effectiveness of multipass and multirow writing methods for massively parallel e-beam systems

Cite as: J. Vac. Sci. Technol. B 38, 062601 (2020); doi: 10.1116/6.0000547
Submitted: 13 August 2020 · Accepted: 18 September 2020 ·
Published Online: 2 October 2020



Md Nabid Hasan,[1] Soo-Young Lee,[1,a)] Byung-Sup Ahn,[2] Jin Choi,[2] and Joon-Soo Park[2]

## AFFILIATIONS

[1]Department of Electrical and Computer Engineering, Auburn University, Auburn, Alabama 36849
[2]Samsung Electronics, Mask Development Team, 16 Banwol-Dong, Hwasung, Kyunggi-Do 18448, South Korea

**Note:** This paper is part of the collection: Electron, Ion, and Photon Beam Technology and Nanofabrication, EIPBN 2020.
[a)]**Electronic mail:** leesooy@eng.auburn.edu

## ABSTRACT

Massively parallel electron-beam systems are equipped with a large number of beams to improve the writing throughput. It is unavoidable that some of the beams are abnormal, e.g., always on or off, spatial and temporal fluctuations of beam current, beam-positioning error, etc. A practical approach to improve the writing quality is to spread the negative effects of abnormal beams spatially. The *multirow writing* (MRW) was introduced, which uses each beam to expose pixels over multiple rows in each writing path minimizing the localization of pixels affected by an abnormal beam. In another method, the *single-row writing* (SRW), each beam exposes pixels in one row in each writing path localizing the affected pixels in a row. To spread the negative effects, especially for the single-row writing, each row of pixels may be exposed through multiple passes, i.e., *multipass writing*. In this study, the multirow and multipass writing methods in various combinations with the MRW and SRW are compared in terms of their effectiveness in reducing the negative effects of abnormal beams. The results from an extensive simulation study are analyzed in detail.



## I. INTRODUCTION

The electron-beam (e-beam) lithography (EBL) is capable of writing patterns in the resist with high resolution and has been utilized in the fabrication of photomasks, imprint lithography molds, experimental circuit patterns, etc.[1–5] However, the main disadvantage of EBL is low throughput, which limits its applicability in the fabrication of large-scale photomasks. E-beam lithographic systems with multiple beams were introduced for improving the writing throughput significantly.[6,7] A massively parallel electron-beam system (MPES) (e.g., Multi-Beam Mask Writer-1000[8]) is equipped with a large number of beams. In such a system, it is highly likely that some beams are defective, e.g., always-off or always-on faulty beams, spatial and temporal fluctuations in beam current, and beam-positioning error. Hence, it is crucial to develop an optimal writing method, which can minimize the adverse effects on the writing quality.

Several writing methods have been introduced for the MPES. In the single-row writing,[9] each pixel may be exposed by one beam (SRW-I) or a group of beams (SRW-II). In both methods, a beam is confined to exposing a single row, which makes the effects of abnormal beams localized in the respective rows. The multipass (MP) writing[10] can be employed in both SRW methods, i.e., SRW-I-MP and SRW-II-MP. However, it requires each writing path to be exposed multiple times and a positional shift of the substrate in the scanning direction in each pass. An important issue is to determine the number of passes and the amount of shift in each writing path, which maximizes the effectiveness of the multipass writing. In the multirow writing (MRW),[11] a beam exposes pixels from multiple rows in each writing path to spread affected pixels and decrease the number of times a pixel is exposed by a beam. In our previous study,[12] through an extensive simulation, the effects of abnormal beams on the writing qualities such as exposure variation, line edge roughness (LER), and maximum indent were analyzed, and the MRW was shown to perform better than the SRW-I and the SRW-II. What remains to be determined in the MRW is the optimal spatial distribution of pixels to be exposed by each beam. Also, no study has been done on the comparison of the writing qualities of the MP writing and MRW in case of different beam abnormalities.

The main objectives of this study are to derive general procedures to find the optimal MP writing and MRW, which minimize the effect of abnormal beams in an MPES, and to compare the SRW-I-MP, SRW-II-MP, MRW-MP methods through an extensive simulation in terms of the above-mentioned writing qualities. The beam abnormalities considered in this study are always-off faulty beams, spatial and temporal fluctuations in beam current, and beam-positioning error.

The rest of the paper is organized as follows. In Sec. II, the exposure process in the massively parallel e-beam system is described. In Sec. III, the general procedures to find the optimal multipass writing and the optimal multirow writing method are described. In Sec. V, the simulation setup is explained along with the quality metrics. In Sec. VI, the simulation results are discussed, followed by a summary in Sec. VII

## II. MODEL

A model of MPES is employed in this simulation study, which is derived from eMET[13] and MBM-1000.[14] A number of beams are arranged in a 2D array, where the cross section of a beam is a square of $B \times B$. Each beam can be turned on or off individually, and beams are deflected in a synchronized manner, i.e., the same angle and direction. In this section, the coordinate and substrate systems employed in this study are depicted and the exposure process in the MPES is described along with the modeling of the transfer function. The effects of different beam abnormalities, i.e., always-off faulty beams, spatial and temporal fluctuation in beam currents, and beam-positioning error, on the exposure distribution are also explained.

### A. Exposure process

It is assumed in this study that the resist layer of a substrate system is on the X–Y plane and parallel beams are in the Z direction, i.e., normal to the X–Y plane, as illustrated in Fig. 1. The resist layer to be exposed can be modeled as an array of square-shaped pixels with size $B \times B$, the same as the beam size on the substrate (Fig. 1). Rows and columns of pixels or beams are in the X and Y dimensions, respectively. The exposing interval, $I_{ex}$, can be larger, smaller, or equal to $B$. For simplicity, it is assumed that $I_{ex} = B$ throughout this paper.

The 3D transfer function is denoted by $TF(x, y, z)$, describing the exposure distribution in the resist when a point (pixel) is exposed by a beam. Then, the 3D spatial distribution of exposure, $E(x, y, z)$, can be expressed by the following convolution:

$$E(x, y, z) = \int_{y'} \int_{x'} d(x - x', y - y') TF(x', y', z)\, dx'\, dy', \qquad (1)$$

where $d(x, y)$ represents the dose distribution given by all beams.

### B. Transfer function

An ideal TF may be defined to be constant within the area of $B \times B$ and zero outside for all layers of resist. However, a real TF deviates from the ideal one due to the beam blur and the electron scattering in the resist layers.[8] The TF is modeled by the convolution of the ideal TF and a Gaussian function as shown in Fig. 2.[12] The standard deviation $\sigma_t$ of the Gaussian function, to be referred to as blurring factor, quantifies the level of beam blur and electron scattering.[15] The blurring factor depends on several parameters such as resist type, resist thickness, beam energy, beam size, etc. A smaller $\sigma_t$ results in a transfer function closer to the ideal one and leads to a lower level of proximity effect.

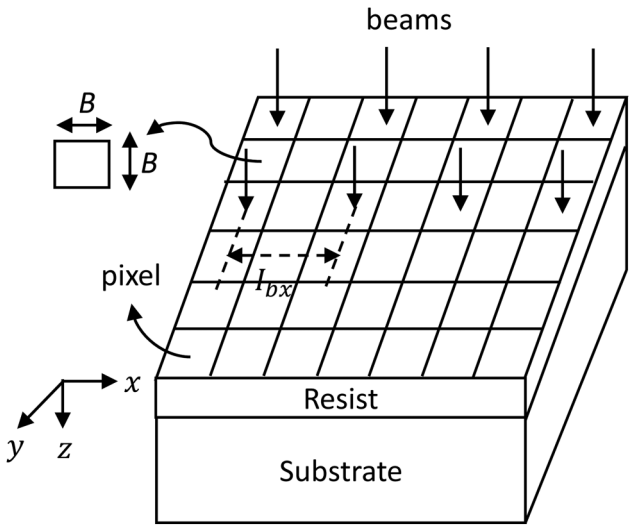


**FIG. 1.** Substrate moves in the $x$-direction exposed by parallel beams: the beam size is $B \times B$, and the beam interval is $I_{bx}$.

### C. Abnormal beams

In analyzing the writing qualities of different writing methods, the beam abnormalities of always-off faulty beams, spatial and temporal fluctuations of beam current, and beam-positioning error are considered.

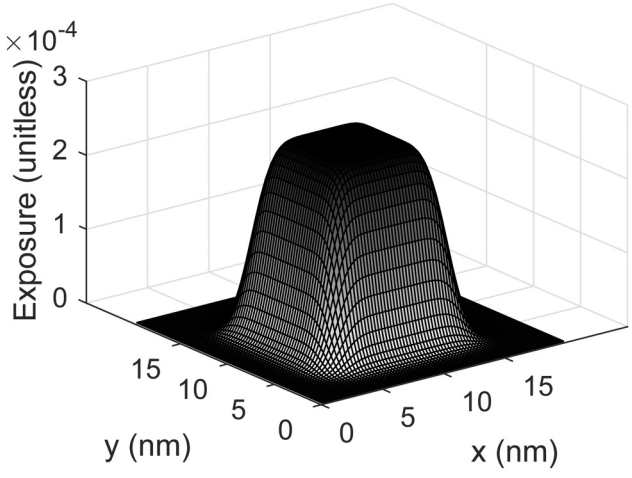


**FIG. 2.** 3D view of the transfer function with $B = 10$ nm and $\sigma_t = 2$ nm.

### 1. Always-off faulty beams

The probability of a beam being faulty is very low, e.g., 0.05%, in an MPES. However, due to the large number of beams, there would be always a few defective beams (statistically distributed), of which the beam currents are lower than normal. Such beams are considered to be always-off in the simulation.

### 2. Spatial fluctuation of beam current

As electrons travel from the electron source to the 2D array of beam apertures, they experience blurring, which results in a high beam current density in the center of the aperture array and a gradually decreasing beam current density away from the center. This distribution of beam currents may be modeled by clipping a square array from the center of a 2D Gaussian distribution as shown in Fig. 3(a). The value associated with each element $(i, j)$ of the array represents the current of beam $(i, j)$. The standard deviation $\sigma$ of all the beam currents represents the level of spatial fluctuation.

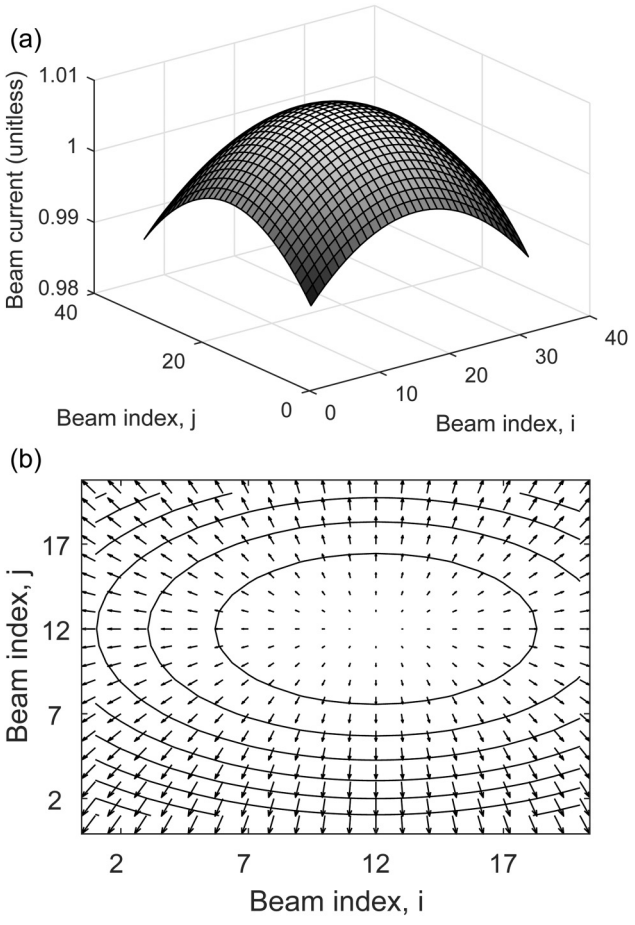


**FIG. 3.** Beam abnormalities: (a) an example of the spatial fluctuation of beam currents, where the doses given by the beams are slowly decreasing from the center of the aperture array, and (b) a vector field of the beam-positioning error guided by the concentric ellipses, $ax^2 + by^2 = 1$, where $a$ and $b$ are varied.

### 3. Temporal fluctuation of beam current

The current of a beam may vary (fluctuate) with time. To exclude the spatial fluctuation, it is assumed that the temporal fluctuation is the same for all beams. In this study, the case where the beam current slowly drifts is considered, i.e., the current (dose) of a beam increases linearly in each step from a minimum to a maximum value. The standard deviation $\sigma$ of the dose given by a beam in each step over the entire exposing process is used to represent the level of temporal fluctuation.

### 4. Beam-positioning error

The actual point of exposure of a beam may deviate from its target position, in both $x$ and $y$ directions, due to the imperfect deflecting electric and magnetic fields. The deviation of each beam, i.e., beam-positioning error, may be expressed by a vector $(\delta x, \delta y)$. While various spatial distributions of beam-positioning error may be considered, this study deals with only a spatially correlated beam-positioning error, which may be modeled to follow a parameterized function. The vector field of beam-positioning error shown in Fig. 3(b), considered in this study, is generated based on the equation of ellipse $ax^2 + by^2 = 1$ where $a$ and $b$ are varied. The standard deviation $\sigma$ of $\delta r = \sqrt{\delta x^2 + \delta y^2}$ among all beams represents the overall level of beam-positioning error.

## III. OPTIMIZATION OF WRITING METHODS

The writing methods, single-row writing-I (SRW-I), single-row writing II (SRW-II), and MRW, were proposed previously.[9,11] In a *step*, a beam gives a unit dose of $d$ to a pixel. In the single-row writing method (SRW-I or SRW-II),[9] the writing path of each beam is confined to a single row of pixels. As the substrate is moved in the $X$ dimension during the exposing process, each beam follows a pixel, being deflected in each step, to give a total dose of $D = n_s d$ to the pixel through a *cycle* of $n_s$ steps. After that, the beam is directed to another pixel in the next cycle. The beam interval, $I_{bx}$, is considered to be an integer multiple of $B$, i.e., $I_{bx} = mB$. Here, $m$ is to be $n_s - 1$, which ensures a uniform dose over $(n_s)$ contiguous pixels through a run of $n_s$ cycles. In the SRW-II, each pixel is exposed jointly by a group of $n_g$ consecutive beams, instead of a beam as in the SRW-I. In the MRW,[11] the writing path of each beam is over multiple rows of pixels and each pixel is exposed by a beam only once. That is, each beam exposes a set of $n_s$ pixels, each pixel once, distributed over multiple rows. If the target dose for a pixel is $D = n_s d$, each pixel is exposed by $n_s$ different beams in a row. There are more than one way of selecting a set of $n_s$ pixels over multiple rows, where the set is referred to as *pattern*. A basic requirement for a pattern to achieve a uniform dose is *stackability*,[11] that is, being able to replicate and stack the pattern in the $X$ dimension without a hole or overlap.

In order to optimize the writing qualities, the effect of abnormal beams needs to be spread maximally. The procedure to minimize the localization of pixels affected by abnormal beams is described for each of the MP writing and MRW in the following. In both cases, it is assumed that $n_s = \frac{I_{bx}}{B} + 1 = 4$ and the exposing interval, $I_{ex} = B$.

The positional shift, $\Delta x$, in the MP writing is defined as the absolute amount of positional shift in the direction of the substrate after each pass. The number of passes is denoted by $n_p$.

### A. Multipass writing

In the MP writing, the effect of abnormal beams is delocalized by increasing the number of passes $n_p$ with a positional shift $\Delta x$ of the substrate. The relation between $n_p$ and $\Delta x$ required for the optimal MP writing needs to be determined. In Fig. 4, two different realizations of the MP writing with the SRW-I method are illustrated. When $\Delta x = B$ as in Fig. 4(a), all pixels in the writing path are exposed by each beam through $n_s$ passes. Increasing $n_p$ beyond $n_s$ results in certain pixels exposed by the same beam more than once. If that beam is defective, the negative effect on those pixels will be larger. Hence, the optimal number of passes in this case is $n_s$. When $\Delta x = 2B$ as in Fig. 4(b), every other pixel is exposed by the same beam once after $\frac{n_s}{2}$ passes. Increasing $n_p$ beyond $\frac{n_s}{2}$ results in specific pixels exposed by the same beam twice. Therefore, in general, when $\Delta x = nB$, the optimal number of passes is $n_s/n$ where $n$ is an integer. However, when $\Delta x = B$, the negative effect of an abnormal beam is spread most (to the entire row of pixels) with $n_s$ passes. Therefore, when $\Delta x = B$ and $n_p = n_s$, the MP writing is optimized.

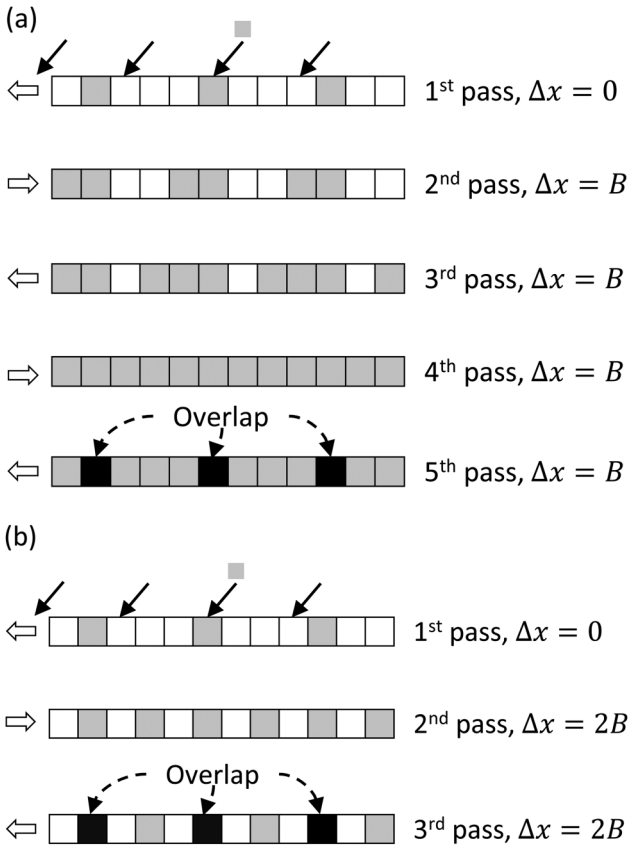


**FIG. 4.** Illustration of the pixels exposed by a beam in the MP writing where (a) $\Delta x = B$ and (b) $\Delta x = 2B$. The gray pixels represent the pixels exposed once by the beam with a small gray square on its top. The black pixels represent the pixels exposed by the same gray beam more than once. In both cases, $n_s = 4$ and $I_{bx} = 3B$.

### B. Multirow writing

An optimal MRW pattern needs to be selected such that the distance among the pixels exposed by the same beam is maximized. In this way, the localization of pixels affected by an abnormal beam is minimized. Let $(\Delta H, \Delta V)$ denote the displacement vector, where $\Delta H$ and $\Delta V$ represented in pixel are the horizontal and vertical displacements between the two pixels exposed consecutively by a beam (assuming that pixels in a pattern are exposed from the top to bottom row of the pattern). Also, $(\Delta X, \Delta Y)$ denotes the displacement vector between the two closest pixels exposed by the same beam at the completion of exposing process. The larger the $\sqrt{\Delta X^2 + \Delta Y^2}$ is, the less the localization of affected pixels is. In Fig. 5, four different MRW patterns for $n_s = 4$ and $I_{bx} = 3B$ are shown. In all patterns, $\Delta V = 1$ to achieve the stackability in one pass. When $\Delta H$ is less than $\frac{n_s}{2}$ as in Fig. 5(a) or greater than $\frac{n_s}{2}$ as in Fig. 5(b), $\Delta X$ is less than $\frac{n_s}{2}$. On the other hand, when $\Delta H = \frac{n_s}{2}$ as in the patterns of Figs. 5(c) and 5(d), $\Delta X = \frac{n_s}{2}$. Hence, when $\Delta H = \frac{n_s}{2}$, the distance $\sqrt{\Delta X^2 + \Delta Y^2}$ is maximized. Therefore, in general, the MRW pattern with $\Delta H = \frac{n_s}{2}$ performs better than any other MRW patterns.

Let $W_p$ denote the width of a pattern represented in pixel. The two patterns in Figs. 5(c) and 5(d) have the same $\Delta H = \frac{n_s}{2}$, but different $W_p$, i.e., $W_p = \frac{n_s}{2} + 1 = 3$ in the former pattern and $W_p = 3\frac{n_s}{2} + 1 = 7$ in the latter pattern. Therefore, the deflection angles of beams to realize the pattern in Fig. 5(c) are smaller. Also, the exposing time is shorter for the pattern of Fig. 5(c) compared to the pattern in Fig. 5(d), where the initial and final latencies of exposing a feature are longer. Hence, the optimal MRW pattern is obtained when $\Delta H = \frac{n_s}{2}$ and $W_p = \frac{n_s}{2} + 1$.

## IV. QUALITY METRICS

The defective beams in an MPES can cause a significant deviation from the desired spatial distribution of exposure leading to a rough feature boundary. In evaluating the writing quality, a few metrics are considered, i.e., exposure variation within a feature, LER, and maximum indent.

### A. Exposure variation

The exposure variation is quantified as the standard deviation of exposure within a feature at a certain resist layer, $z = z_i$ [Fig. 6(a)] normalized to the average exposure,

$$SD_E = \frac{1}{\overline{E}(z_i)} \sqrt{\frac{1}{wl} \sum_{y=0}^{l} \sum_{x=0}^{w} [E(x, y, z_i) - \overline{E}(z_i)]^2}, \tag{2}$$

where $\overline{E}(z_i) = \frac{1}{wl} \sum_{y=0}^{l} \sum_{x=0}^{w} E(x, y, z_i)$ is the average exposure, and $w$ and $l$ are the width and length of a feature, respectively.

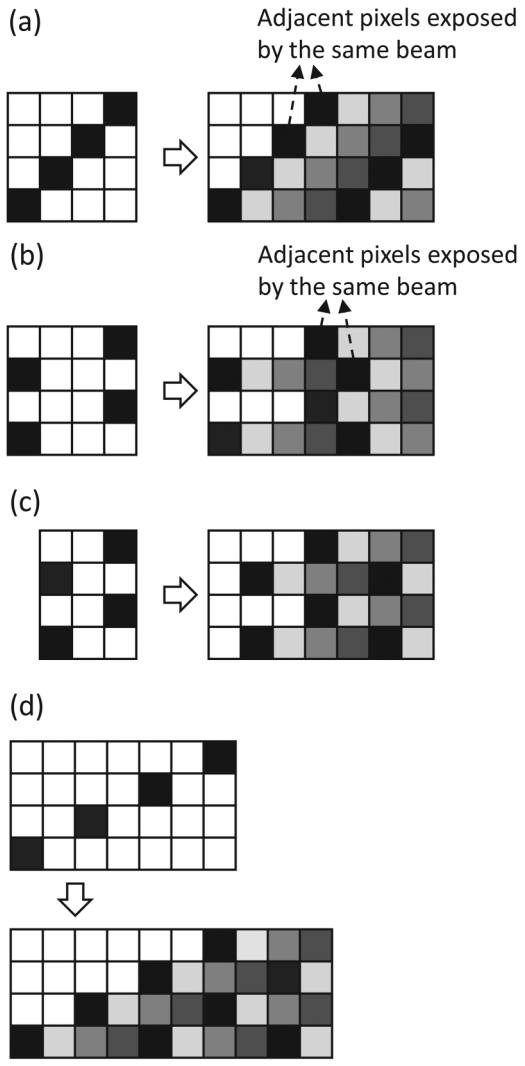


**FIG. 5.** Different realizable patterns for the MRW with $n_s = 4$ and $l_{bx} = 3B$, where (a) $\Delta H = 1$ and $W_p = 4$, (b) $\Delta H = 3$ and $W_p = 4$, (c) $\Delta H = 2$ and $W_p = 3$, and (d) $\Delta H = 2$ and $W_p = 7$. In all cases, $\Delta V = 1$.

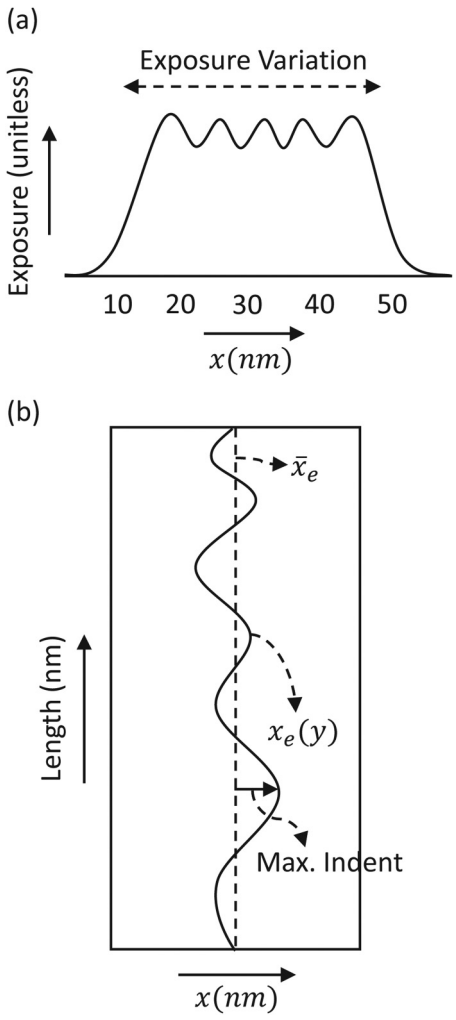


**FIG. 6.** Metrics of writing quality: (a) exposure variation and (b) LER and maximum indent. The LER is computed as the standard deviation of edge location $x_e(y)$ (solid) and the maximum indent is the largest distance inward to the edge from the average edge location $x_e$ (dashed). The left boundary of a line feature is shown and the feature size is $40 \times 120\,\text{nm}^2$.

Such quantification can be dominated by the exposure drop over the feature boundary. Therefore, the exposure drop over the feature boundary is excluded while calculating the exposure variation.

### B. Line edge roughness

The LER is defined as the standard deviation of edge location along the length dimension of a feature, which can be expressed as follows [Fig. 6(b)]:

$$\text{LER} = \sqrt{\frac{1}{l}\sum_{0}^{l}(x_e(y) - \bar{x}_e)^2}, \tag{3}$$

where $x_e(y)$ is the edge location and $\bar{x}_e$ is the average edge location, i.e., $\bar{x}_e = \frac{1}{l}\sum_0^l x_e(y)$ at a resist layer.

### C. Maximum indent

Always-off faulty beams may introduce an exposure drop near the feature boundary, which can cause a large indent increasing the resistance of a signal path directly. Hence, the maximum indent is an important metric. It is measured as the distance from the average edge location to the farthest edge location inward [Fig. 6(b)]. The maximum indent $(\Delta x_{in})_{max}$ can be represented as

$$(\Delta x_{in})_{max} = \max_y(\,|\,x_{e,in}(y) - \bar{x}_e\,|\,), \tag{4}$$

where $x_{e,in}(y)$ is the edge location inside the average feature boundary.

## V. SIMULATION

A single line feature of width 100 nm and length 500 nm is exposed by the MPES along its width dimension on a typical substrate system. The resist is modeled by five layers to consider the layer dependency of exposure. The beam cross section at the surface of resist is $10\,\text{nm} \times 10\,\text{nm}^2$ ($B = 10\,\text{nm}$). Therefore, the exposing interval $I_{ex} = B = 10\,\text{nm}$. All the pixels are given the dose $D = 10d$ ($n_s = 10$). The number of beams in a set is 10 and the beam interval $I_{bx} = 9B = 90\,\text{nm}$ ($n_s = \frac{I_{bx}}{B} + 1$). For the SRW-II, $n_g$ is set to 2.

The TF is modeled based on the 3D point spread function (PSF) generated using a Monte Carlo simulation program CASINO (Ref. 16) for the substrate system of 100 nm PMMA on Si, the beam energy of 50 keV, and the beam diameter of 6 nm. The total exposure and forward scattering range (the standard deviation of Gaussian) are extracted from the PSF in each of the five resist layers. The ratios of the total energy and forward scattering range among the five resist layers are referred to in setting the total exposure and $\sigma_t$ of the Gaussian function used to generate the TF of each layer.

The 3D exposure distribution in the resist is computed at the resolution $I_{sm}$, referred to as *simulation interval*, which is set to $\frac{1}{2}\,nm$. The exposure variation is calculated from the exposure distribution. The developing-rate distribution is obtained from the exposure distribution and then the remaining resist profile is obtained through a fast path-based simulation of resist development.[17] The development simulation continues until the resist is fully developed to the bottom layer. The total dose is set such that the CD of developed feature at the middle layer without considering the beam abnormalities is as close to the target CD as possible. To measure the LER and maximum indent, the middle 80% segment of the developed feature along the length dimension is considered to exclude the edge effect (corner rounding). All the quality metrics are averaged over simulation runs of ten typical cases.

To expose the feature used in this simulation, a relatively small number of beams is required. In this case, the number of faulty beams $n_f$ is likely to be 0, since the faulty rate is very low in an MPES. Therefore, in the simulation of always-off faulty beams, the effect of a varying number of faulty beams $n_f$, rather than a faulty rate, is considered, where $n_f$ is varied from 0 to 5. In the simulation of the spatial and temporal fluctuations of beam current, $\sigma$ is varied from 0.5% to 20%, where the maximum fluctuation is limited to 40% of the average current (or dose per step). The standard deviation of beam-positioning error is changed from 0 to 1 nm with a maximum deviation of 5nm from the target position.

## VI. RESULTS AND DISCUSSION

In this section, the results are presented in three parts. First, three different implementations of the MP writing in the SRW-I, i.e., SRW-I-MP, are compared. Then, simulation results for two different patterns of the MRW are discussed. Finally, the results from an extensive simulation comparing the SRW-I, SRW-II, and MRW with and without the MP writing are presented.

### A. Multipass writing

The three quality metrics, e.g., exposure variation, LER, and maximum indent, obtained with $n_f$ varied are provided in Fig. 7 for three different implementations of the SRW-I-MP, i.e., ($n_p = 10$, $\Delta x = B$), ($n_p = 5$, $\Delta x = 2B$), and ($n_p = 2$, $\Delta x = 5B$). In the SRW-I-MP with $n_p = 10$ and $\Delta x = B$, each beam exposes all the pixels in a row. Hence, each pixel is exposed by all of the ten beams in a set. Consequently, the dose reduction due to a faulty beam is $d$. For $n_p = 5$ and $\Delta x = 2B$, each pixel is exposed by five different beams in a set and the dose reduction due to a faulty beam is $2d$. Similarly, since each pixel is exposed by two different beams when $n_p = 2$ and $\Delta x = 5B$, the dose reduction due to a faulty beam is $5d$. Therefore, the smallest dose reduction occurs when $n_p = 10$ and $\Delta x = B$. Hence, the SRW-I-MP with $n_p = n_s$ and $\Delta x = B$ gives the best result in terms of the quality metrics.

In Fig. 8, the level of spatial fluctuations of beam current is varied for three different implementations of the SRW-I-MP. The quality metrics are improved most when $n_p = 10$ and $\Delta x = B$. This is because, in this case, each pixel is exposed by a larger number of beams than the other implementations and, therefore, different doses from multiple beams have a better chance to be averaged out. For the same reason, the SRW-I-MP with $n_p = 10$ and $\Delta x = B$

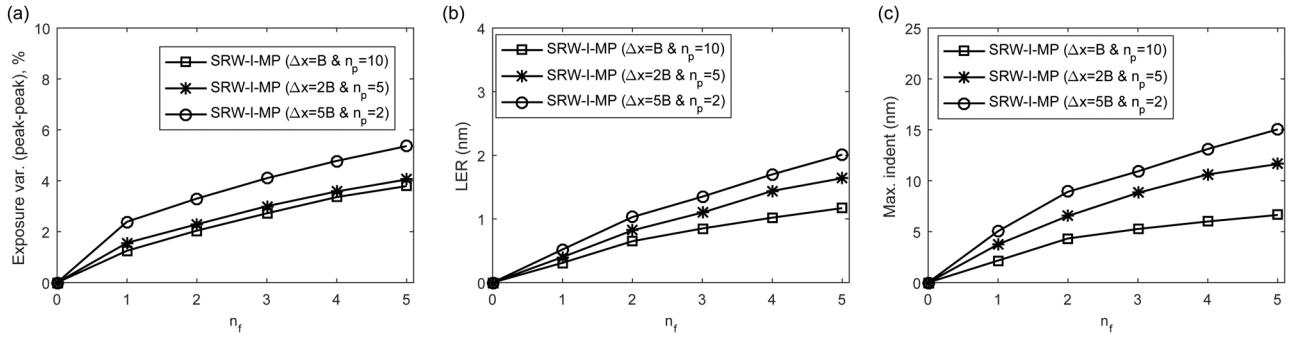


**FIG. 7.** (a) Exposure variation, (b) LER, and (c) maximum indent with the number of always-off faulty beams ($n_f$) varied. $\sigma_t = 2\,\text{nm}$.

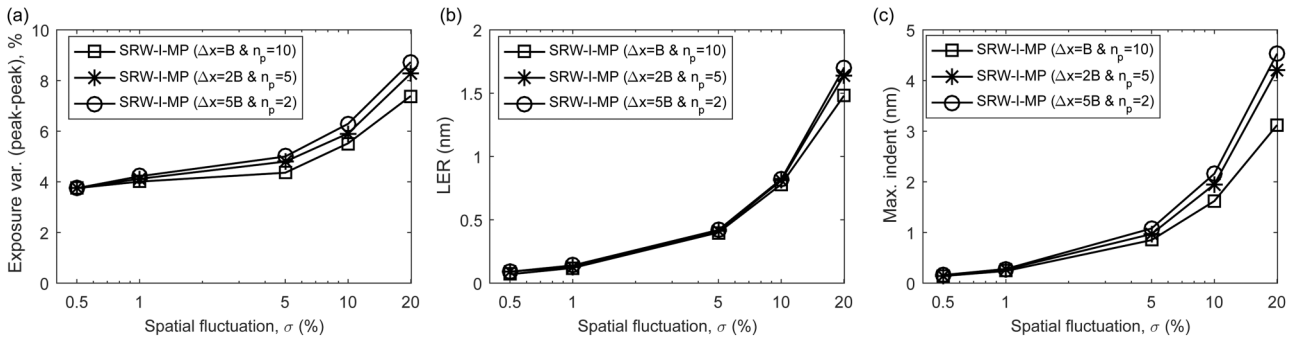


**FIG. 8.** (a) Exposure variation, (b) LER, and (c) maximum indent with the spatial fluctuation ($\sigma$) of beam current varied. $\sigma_t = 2$ nm, $n_f = 0$.

gives the best results in the case of the beam-positioning error, as shown in Fig. 9.

The three quality metrics for the varying level of temporal beam-current fluctuation are plotted in Fig. 10. For a fixed $\sigma$ of the temporal fluctuation, the difference between the initial and final beam currents (of a beam), $\Delta I$, is the same for all beams. In the MP writing, the higher the $n_p$, the larger the total number of steps. Since $\Delta I$ is the same independent of $n_p$, the current increment per step is inversely proportional to $n_p$. As the variation of beam current with time decreases with increasing $n_p$, the difference between the minimum and maximum doses in pixels along the boundary of a feature decreases with increasing $n_p$. Therefore, the SRW-I-MP with the highest $n_p$ ($n_p = 10$) has the smallest exposure variation, LER, and maximum indent.

## B. Multirow writing

The optimal pattern of the MRW ($\Delta H = \frac{n_s}{2} = 5$ and $W_p = \frac{n_s}{2} + 1 = 6$) is compared with another pattern ($\Delta H = 1$ and $W_p = n_s = 10$) in the cases of always-off faulty beams, spatial and temporal fluctuations of beam current, and beam-positioning error. From the results shown in Figs. 11–14, it is observed that the optimal pattern improves the quality metrics significantly. The results for the MRW with the pattern $\Delta H = \frac{n_s}{2}$ and $W_p = \frac{n_s}{2} + 1$ combined with the optimal MP writing ($\Delta x = B$ and $n_p = n_s$) are also presented. In all cases, the MRW-MP improves the quality metrics most.

The dose reduction due to an always-off faulty beam is $d$ in any realizable MRW pattern. When $(\Delta H, \Delta V) = (1, 1)$, adjacent pixels are affected. But, when $(\Delta H, \Delta V) = (5, 1)$, an affected pixel is surrounded by nonaffected pixels, which can compensate for the dose reduction in the affected pixel. Therefore, the exposure variation for the pattern $(\Delta H, \Delta V) = (5, 1)$ is smaller than that for the pattern $(\Delta H, \Delta V) = (1, 1)$, resulting in smaller LER and maximum indent as can be seen in Fig. 11. In the optimal MRW-MP, each beam exposes all the pixels in its writing path of ten rows in ten passes. Hence, each pixel is exposed by ten times as many beams as in the MRW. Consequently, the amount of dose reduction due to a faulty beam is reduced ten times. Therefore, the MRW-MP improves the exposure variation, LER, and maximum indent significantly compared to the MRW.

Figure 12 shows that the optimal MRW pattern performs better than the pattern with $\Delta H = 1$ in the case of spatial fluctuation of beam current. In the optimal MRW pattern with $(\Delta H, \Delta V) = (5, 1)$, the distance between two pixels exposed by the same beam is maximized. The pixels between the two affected

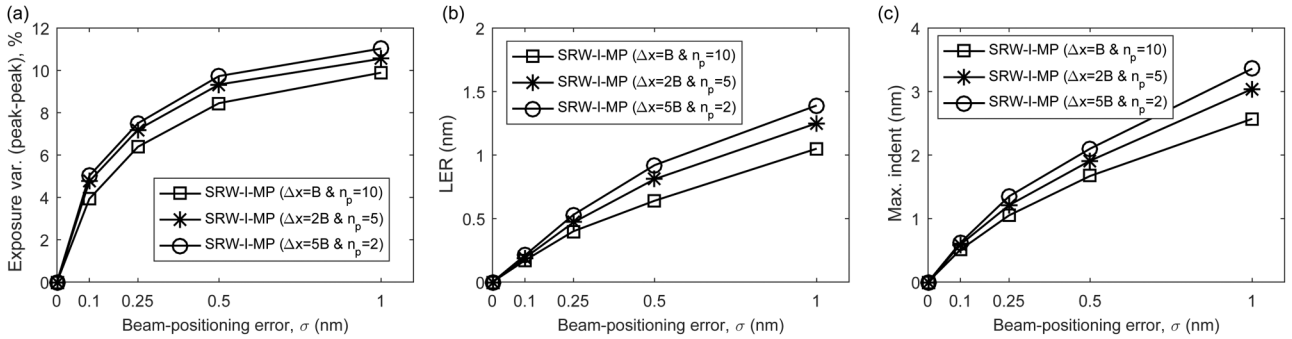


**FIG. 9.** (a) Exposure variation, (b) LER, and (c) maximum indent with the beam-positioning error ($\sigma$) varied. $\sigma_t = 2$ nm, $n_f = 0$.

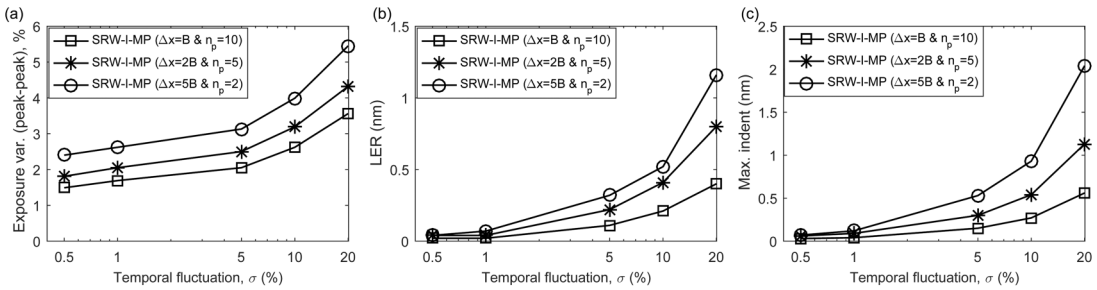


**FIG. 10.** (a) Exposure variation, (b) LER, and (c) maximum indent with the temporal fluctuation ($\sigma$) of beam current varied. $\sigma_t = 2$ nm, $n_f = 0$.

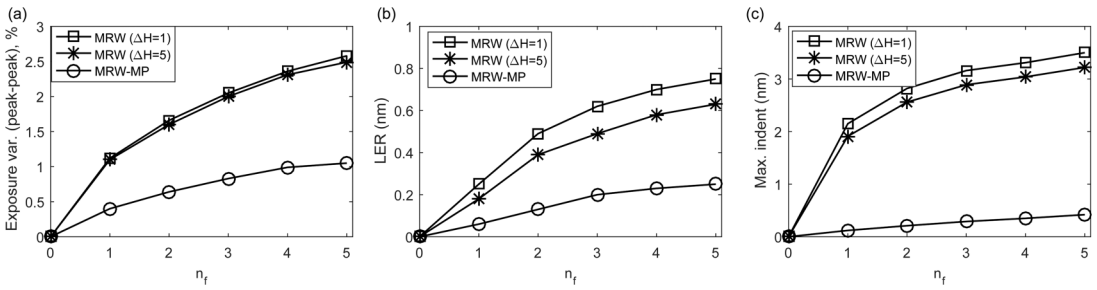


**FIG. 11.** (a) Exposure variation, (b) LER, and (c) maximum indent with the number of always-off faulty beams ($n_f$) varied. $\sigma_t = 2$ nm.

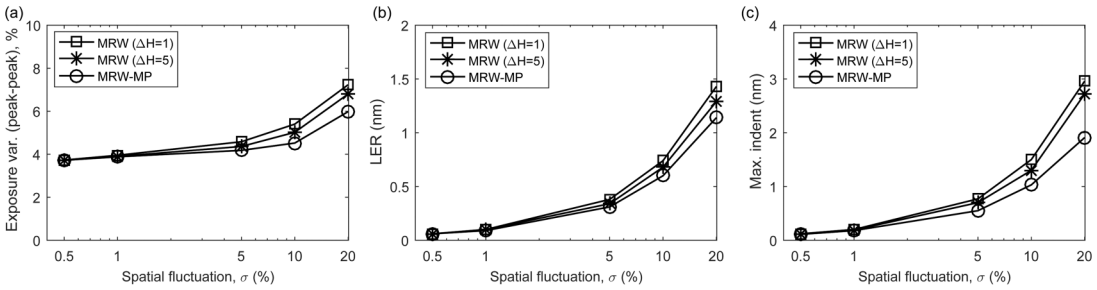


**FIG. 12.** (a) Exposure variation, (b) LER, and (c) maximum indent with the spatial fluctuation ($\sigma$) of beam current varied. $\sigma_t = 2$ nm, $n_f = 0$.

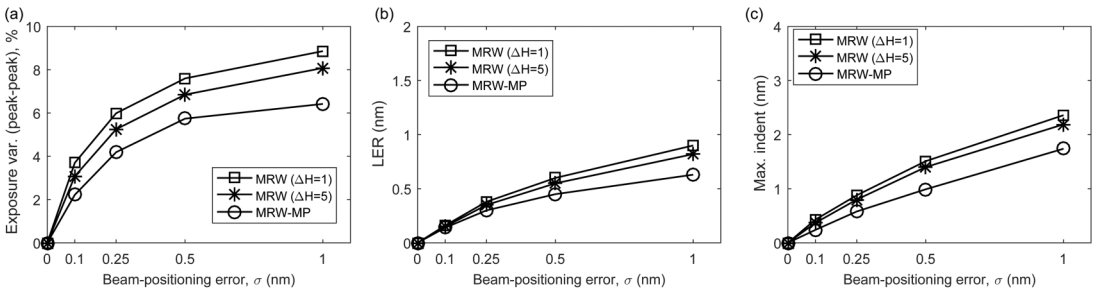


**FIG. 13.** (a) Exposure variation, (b) LER, and (c) maximum indent with the beam-positioning error ($\sigma$) varied. $\sigma_t = 2$ nm, $n_f = 0$.

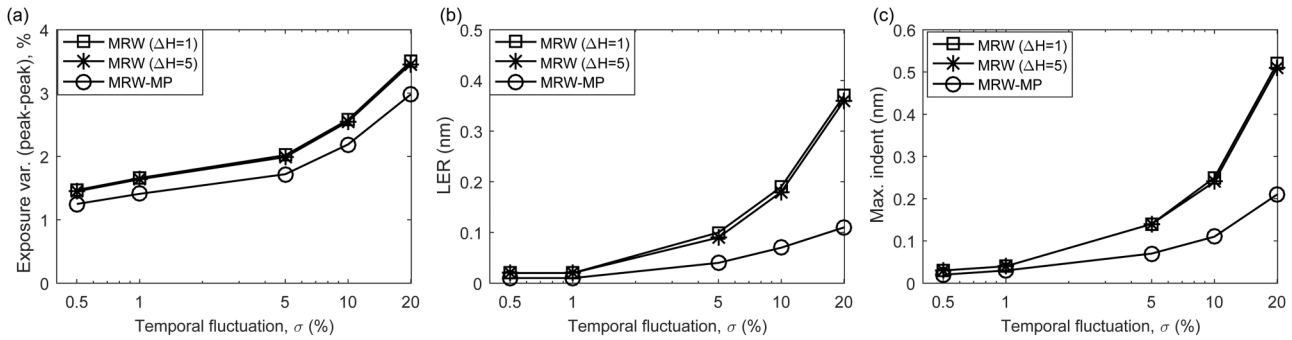


**FIG. 14.** (a) Exposure variation, (b) LER, and (c) maximum indent with the temporal fluctuation ($\sigma$) of beam current varied. $\sigma_t = 2$ nm, $n_f = 0$.

pixels are exposed by other beams in the same writing path. On the other hand, when $(\Delta H, \Delta V) = (1, 1)$ in an MRW pattern, adjacent pixels are affected by the same beam, resulting in a lower number of surrounding pixels exposed by other beams. Hence, the averaging effect of spatial fluctuation of beam current is larger in the optimal MRW pattern. In the optimal MRW-MP, each pixel is exposed by all the beams in each writing path. Therefore, the averaging effect is maximized, resulting in the smallest exposure variation, LER, and maximum indent. For the same reasons, similar trends are observed in the case of beam-positioning error as shown in Fig. 13.

The three quality metrics obtained with the temporal fluctuation of beam current varied are provided in Fig. 14. In the MRW, the number of steps required to expose all the pixels in a writing path as well as the current increment per step are the same for both $\Delta H = 1$ and $\Delta H = 5$. As a result, the difference between the minimum and maximum doses in pixels along the boundary of a feature is almost the same in both cases. Therefore, the improvement of the writing quality by the optimal pattern ($\Delta H = 5$) over the nonoptimal pattern ($\Delta H = 1$) is not substantial in the case of temporal fluctuation.

### C. Comparison of the MP writing and MRW

In this comparison study, the optimal MRW pattern with $\Delta H = \frac{n_s}{2}$ and $W_p = \frac{n_s}{2} + 1$ is used. Also, in the SRW-I-MP, SRW-II-MP, and MRW-MP, the optimal MP writing with $n_p = n_s$ and $\Delta x = B$ is applied.

The writing qualities of the SRW-I, SRW-I-MP, SRW-II, SRW-II-MP, MRW, and MRW-MP are compared in the cases of always-off faulty beams (Fig. 15), spatial beam current fluctuations (Fig. 16), temporal beam current fluctuations (Fig. 17), and beam-positioning error (Fig. 18). In all cases, the MRW performs better than the SRW-I-MP and SRW-II-MP. The MRW-MP performs even better than the MRW since each pixel in $n_p$ rows is exposed by all the beams in the writing path. Also, the performance of the SRW-I-MP is identical with that of the SRW-II-MP. This is because, in both cases, each of the pixels in a writing path is exposed by all the beams in that writing path.

The dose reduction due to a faulty beam in the SRW-I-MP, SRW-II-MP, and MRW is $d$. However, the affected pixels are confined to only one row in the SRW-I-MP and SRW-II-MP while they are spread over multiple rows in the MRW. Therefore, even

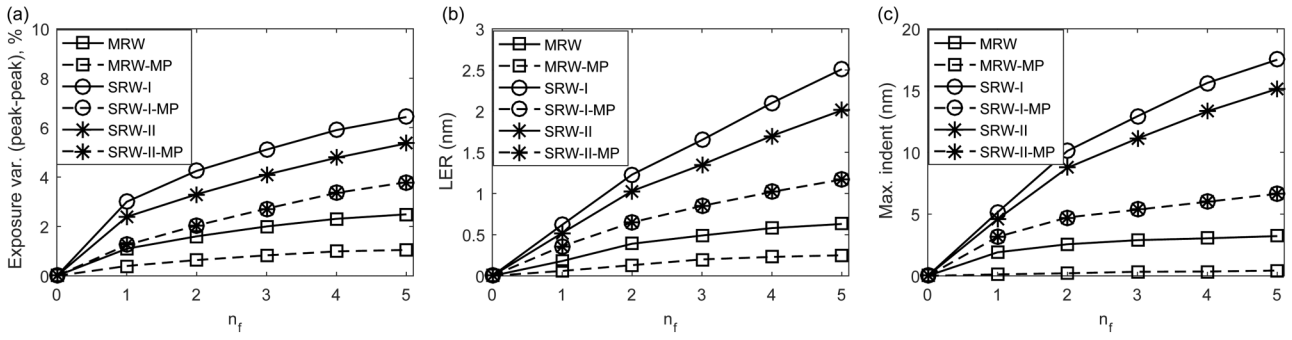


**FIG. 15.** (a) Exposure variation, (b) LER, and (c) maximum indent with the number of always-off faulty beams ($n_f$) varied. $\sigma_t = 2$ nm.

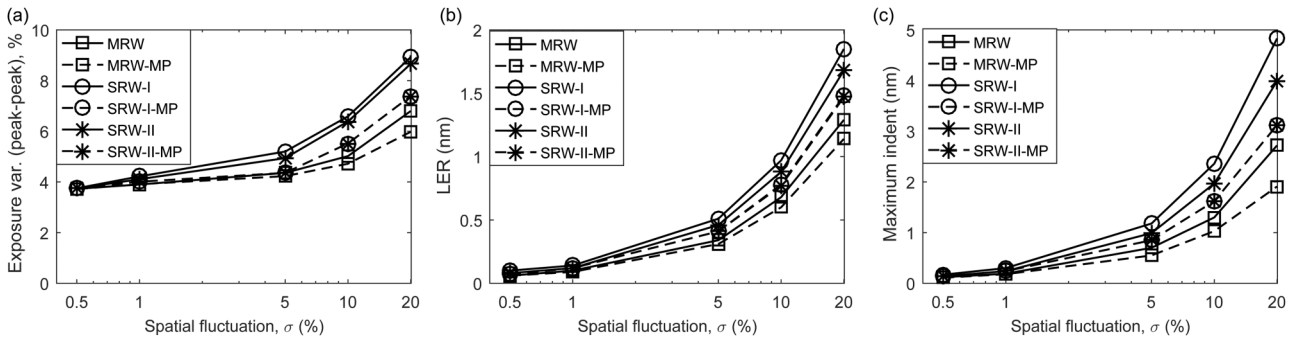


**FIG. 16.** (a) Exposure variation, (b) LER, and (c) maximum indent with the spatial fluctuation ($\sigma$) of beam current varied. $\sigma_t = 2$ nm, $n_f = 0$.

though the dose reduction in an affected pixel is the same, the MRW performs better than the SRW-I-MP and SRW-II-MP in terms of the quality metrics.

In the case of spatial beam-current fluctuation, the higher the number of beams exposing a pixel, the higher the averaging effect of spatial fluctuation of beam current. The number of beams exposing a pixel is the same, i.e., $n_s$, for all of the SRW-I-MP, SRW-II-MP, and MRW, but there is a slight improvement of quality metrics by the MRW compared to the other two (Fig. 16). In the SRW-I-MP or SRW-II-MP, each beam exposes pixels in a single row, while in the MRW, each beam exposes pixels over multiple rows spreading its effect. Therefore, the overall exposure distribution is smoother in the MRW resulting in smaller LER and maximum indent. In the MRW-MP, as each pixel is exposed by each of the $n_s^2$ beams in a writing path, the averaging effect of spatial fluctuation of beam currents is the maximum among all the writing methods. As a result, the quality metrics are improved most by the MRW-MP.

From Fig. 17, it is seen that the quality metrics are similar for the SRW-I and SRW-II when temporal fluctuation of beam current is varied. This is because the number of steps required to expose all the pixels in a writing path of a single row is the same for the SRW-I and SRW-II. In the SRW-I-MP, SRW-II-MP, and MRW, the required number of steps is $n_s$ times ($n_s = n_p$) that of the SRW-I or SRW-II. The current increment per step decreases with the increase in the number of steps, which results in a smaller variation of beam current and improves the quality metrics. On the other hand, in the MRW-MP, the number of steps required to expose all the pixels in a writing path of $n_s$ rows is $n_p$ times ($n_p = n_s$) that of the MRW. Therefore, the improvement in the quality metrics by the MRW-MP is largest.

In the case of the beam-positioning error, the higher the number of beams exposing a pixel, the higher the probability of averaging out the effect of the beam-positioning error. The numbers of beams exposing a pixel in the cases of SRW-I, SRW-II, SRW-I-MP, SRW-II-MP, MRW, and MRW-MP are 1, $n_g$, $n_s$, $n_s$, $n_s$, and $n_s^2$, respectively. As a result, the MRW-MP achieves the best result in terms of the quality metrics (Fig. 18). Although the number of beams exposing a pixel is the same for the SRW-I-MP, SRW-II-MP, and MRW, the performance of the MRW is slightly better (Fig. 18). Each pixel is exposed by $n_s$ consecutive beams in the SRW-I-MP and SRW-II-MP while by one in every $n_s$ beams in the MRW. Since the beam-positioning error is spatially correlated, the beams located close to each other have similar error vectors. Therefore, the averaging effect of beam-positioning error is smaller in the SRW-I-MP and SRW-II-MP than in the MRW.

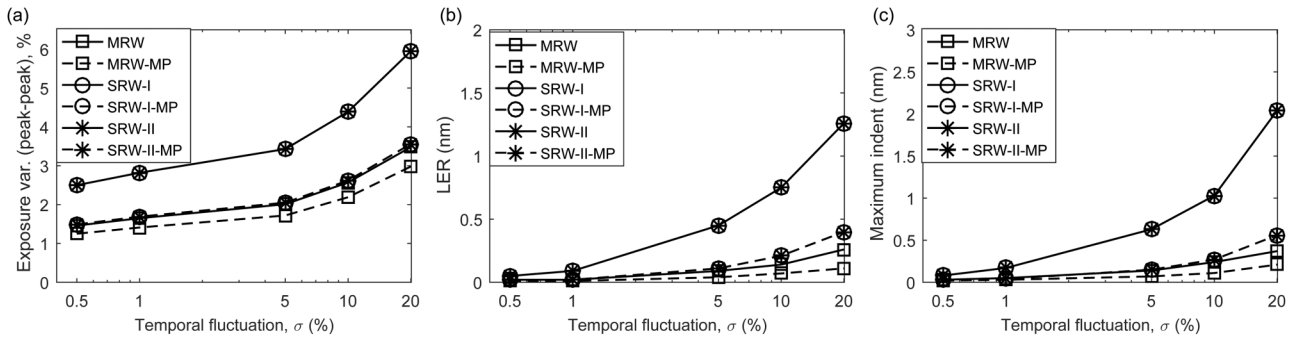


**FIG. 17.** (a) Exposure variation, (b) LER, and (c) maximum indent with the temporal fluctuation ($\sigma$) of beam current varied. $\sigma_t = 2$ nm, $n_f = 0$.

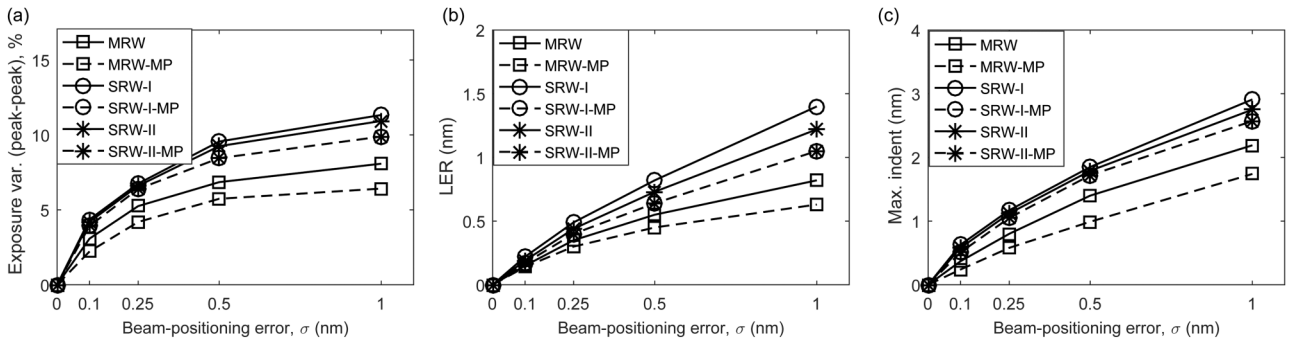


**FIG. 18.** (a) Exposure variation, (b) LER, and (c) maximum indent with the beam-positioning error ($\sigma$) varied. $\sigma_t = 2$ nm, $n_f = 0$.

## VII. SUMMARY

In a MPES, it is likely that some beams are abnormal, possibly affecting the writing qualities substantially. Through an extensive simulation, various combinations of single-row and multirow writing methods along with the multipass writing are compared in terms of their effectiveness in mitigating the negative effect of abnormal beams. The three main objectives of this work are (i) to derive the general conditions for realizing the optimal MP writing and the optimal MRW pattern with a given set of lithographic parameters of a MPES, (ii) to analyze the performances achieved by the optimal MP writing and MRW pattern, and (iii) to compare the SRW-I, SRW-I-MP, SRW-II, SRW-II-MP, MRW, and MRW-MP. The notable results include: (a) the optimal number of passes and positional shift for the MP writing, (b) the optimal writing pattern for the MRW, (c) the optimal SRW and MRW methods achieve significant performance improvements, (d) the MRW (without MP) performs better than the SRW-MP's, and (e) the MRW-MP is superior to all other methods considered in this study. The results from this study may be referred to in designing an effective writing method for current and future MPES's.

## ACKNOWLEDGMENTS

This work was supported in part by a research grant from Samsung Electronics Co., Ltd.

## REFERENCES

[1]S.-Y. Lee and B. D. Cook, IEEE Trans. Semicond. Manuf. **11**, 117 (1998).
[2]S. J. Wind, P. D. Greber, and H. Rothuizen, J. Vac. Sci. Technol. B **16**, 3262 (1998).
[3]M. Osawa, K. Takahashi, M. Sato, H. Arimoto, K. Ogino, H. Hoshino, and Y. Machida, J. Vac. Sci. Technol. B **19**, 2483 (2001).
[4]S.-Y. Lee, S. C. Jeon, J. S. Kim, K. N. Kim, M. S. Hyun, J. J. Yoo, and J. W. Kim, J. Vac. Sci. Technol. B **27**, 2580 (2009).
[5]Q. Dai, S.-Y. Lee, S.-H. Lee, B.-G. Kim, and H.-K. Cho, J. Vac. Sci. Technol. B **30**, 06F307 (2012).
[6]B. J. Lin, J. Micro/Nanolithogr. MEMS MOEMS **11**, 033011 (2012).
[7]P. Petric, C. Bevis, A. Carrol, H. Percy, M. Zywno, K. Standiford, A. Brodie, N. Bareket, and L. Grella, J. Vac. Sci. Technol. B **27**, 161 (2009).
[8]H. Matsumoto, H. Inoue, H. Yamashita, T. Tamura, and K. Ohtoshi, J. Micro/Nanolithogr. MEMS MOEMS **17**, 031205 (2018).
[9]H. Fragner and E. Platzgummer, U.S. patent no. 7 777 201 B2 (17 August 2010).
[10]E. Platzgummer, C. Klein, and H. Loeschner, J. Micro/Nanolithogr. MEMS MOEMS **12**, 031108 (2013).
[11]S.-Y. Lee, B.-S. Ahn, J. Choi, S.-B. Kim, and C.-U. Jeon, J. Vac. Sci. Technol. B **37**, 061602 (2019).
[12]M. N. Hasan, S.-Y. Lee, B.-S. Ahn, J. Choi, S.-B. Kim, and C.-U. Jeon, J. Vac. Sci. Technol. B **37**, 061609 (2020).
[13]C. Klein, H. Loeschner, and E. Platzgummer, J. Micro/Nanolithogr. MEMS MOEMS **11**, 031402 (2012).
[14]H. Matsumoto, H. Yamashita, T. Tamura, and K. Ohtoshi, Proc. SPIE **10454**, 10454E (2017).
[15]T. Kamikubo, K. Ohtoshi, S. Golladay, V. Katsap, R. Kendall, H. Sunaoshi, and S. Tamamushi, Phys. Procedia **1**, 119 (2008).
[16]D. Drouin, A. R. Couture, D. Joly, X. Tastet, V. Aimez, and R. Gauvin, Scanning **29**, 92 (2007).
[17]Q. Dai, R. Guo, S.-Y. Lee, J. Choi, S.-H. Lee, I.-K. Shin, and C.-U. Jeon, Microelectron. Eng. **127**, 86 (2014).